Acid-Base Physiology as CellML Modules

Peter Hunter

Auckland Bioengineering Institute

The following text is designed to go into the tutorial on CellML, OpenCOR and PMR. It may also form the basis of a review paper.

Building multiscale models

Much progress has been made over the last 15 years on establishing model encoding standards (CellML, SBML, FieldML) together with model repositories (PMR, Biomodels) and simulation tools (OpenCOR, *etc.*) based on those standards (refs). CellML also allows a modular approach to model building via imports of separately defined component modules, facilitated by annotation of model variables and parameters so that imported components can be inserted automatically into the composite model (ref). In this section we show how composite multiscale models can be constructed from CellML and FieldML models. We first deal with lumped parameter models based on ODEs and algebraic equations that can be encoded in CellML. The CellML models can be extended to include spatially distributed FieldML models where these are needed.

First, some definitions:

Compartments are well mixed regions of cells, tissues or organs that represent either specific locations or more generic locations that can exist in multiple parts of the body. ***Variables*** are quantities that have units and fixed or variable numeric values and can be associated with compartments. ***Parameters*** are variables with fixed values. ***Models*** contain one or more equations in these variables and can stand alone or be associated with one or more compartments. Note that CellML models require compartments, variables and equations. Until filled with variables and equations, compartments are just empty containers.

Note that the term 'well-mixed' signifies that to an acceptable approximation in the model, the variables within a compartment are distributed homogeneously throughout that compartment. Of course no biological region is perfectly homogeneous and, if necessary, a well-mixed compartment can be replaced by more than one compartment or by a spatially distributed model where concentration gradients are governed by diffusion equations. However, it is often useful to start with a simple lumped parameter compartment model in order to understand basic mechanisms.

Modularity is an important aspect of multiscale modelling and we create composite models by importing other more basic models, as we will demonstrate. *Model reduction* can also be used to simplify a model for computational efficiency. But *model expansion* is equally important - there may be situations where more biophysical detail is called for under certain conditions, or spatial fields need to be considered as part of a model.

Reactions are the binding and unbinding of chemical species (almost always catalysed by an enzyme) and are always reversible under the appropriate conditions. When models include reactions, it is usually with equations that express mass conservation of chemical species and use either first order mass action kinetics or a steady state version in the form of an equilibrium equation. Note that it is often useful in diagrams to show the transfer of mass, energy or information across compartment boundaries and we use arrows

to indicate the movement of variables across compartment boundaries, sometimes with the *flux* (time-varying flow of a variable) written beside the arrow. The direction of these arrows is just for explanatory reasons to show normal directions of movement - the fluxes could be in the reverse direction if conditions allowed it.

The formulation of a model and its encoding in CellML and/or FieldML is a completely separate exercise from the numerical solution of that model. Once a model is formulated it can be solved by any solver that can handle the syntax of the model encoding languages. The verification of the solver is an important but separate issue.

We demonstrate these concepts and how they are supported by CellML and FieldML with the following example of acid-base physiology and the control of pH. Note that some of these models use molecular components while others are treated in a more empirical 'black-box' fashion - possibly to be replaced at a later stage with a more mechanistic model when the physiological data is available to justify this or the questions being asked of the model require this level of detail.

Acid-base physiology

Oxidative metabolism in tissue provides the bulk of the body's energy currency (ATP) by oxidising carbohydrates and fats to carbon dioxide and water. To get rid of this metabolic waste product, CO_2 is transferred from the tissues to the lungs via the blood, primarily in the form of bicarbonate (HCO_3^-) and carried primarily by red blood cells (RBCs). The formation of HCO_3^- from CO_2 via the CO_2 hydration reaction is catalysed by carbonic anhydrase (CA):

$$CO_2 + H_2O \xleftrightarrow{CA} H^+ + HCO_3^-$$

This generates large quantities of H^+ in the blood. Buffering this H^+ - *i.e.* controlling pH within the narrow range compatible with life [1] - requires multiple weak acids and bases to be present in blood [1]. Understanding acid-base physiology therefore requires models of several organs: the muscles (as the major source of metabolism and hence metabolic waste products), the lungs (to exhale CO_2) with the respiratory centre in the mid-brain to control respiration rate, the stomach where acid is excreted to maintain a low pH environment hostile to bacteria, the pancreas (where HCO_3^- is excreted to neutralise stomach acid passed in the chime to the small intestines), the kidneys (to recover filtered HCO_3^-, generate new HCO_3^- and excrete filtered buffers) and the arterial, capillary and venous components of the circulation system (each as homogeneous systems containing blood plasma and RBCs). These six organs or organ systems are illustrated, with their inputs and outputs, in Figure 1.

We follow the physiological approach described in the Boron and Boulpaep textbook on Medical Physiology [1], the models described in Occhipinti and Boron [2] together with earlier publications from the Boron group in Cleveland [3, 4, 5, 6, 7, 8], and models from the Vaughan-Jones and Swietach group in Oxford [9, 10, 11, 12, 13].
We first describe some basic equations that will be used in a number of the models below. The first deals with hydration which, when catalysed by carbonic anhydrase, occurs extremely rapidly with an equilibrium constant

$$K_{CO_2} = \frac{[H^+][HCO_3^-]}{[CO_2]}$$

It is not clear whether the CO_2/HCO_3^- buffering system can be assumed to be in equilibrium, since during rapid changes in pH it may not be, but we make this assumption here and examine the consequences of

[1] Binding proteins are heavily influenced by the dissociation of acidic or basic amino acids, especially histodine, and are therefore dependent on ambient pH. Intracellular metabolism is also influenced by pH - for example, glycolysis and lactic acid formation are inhibited by acidosis (and, conversely, stimulated by alkalosis). K^+ channels in a wide variety of cells are inactivated by acidosis. H^+ affects smooth muscle in blood vessels (vasoconstriction in pulmonary arterioles and vasodilation in the systemic circulation) and reduces Ca^{2+} binding by plasma proteins.

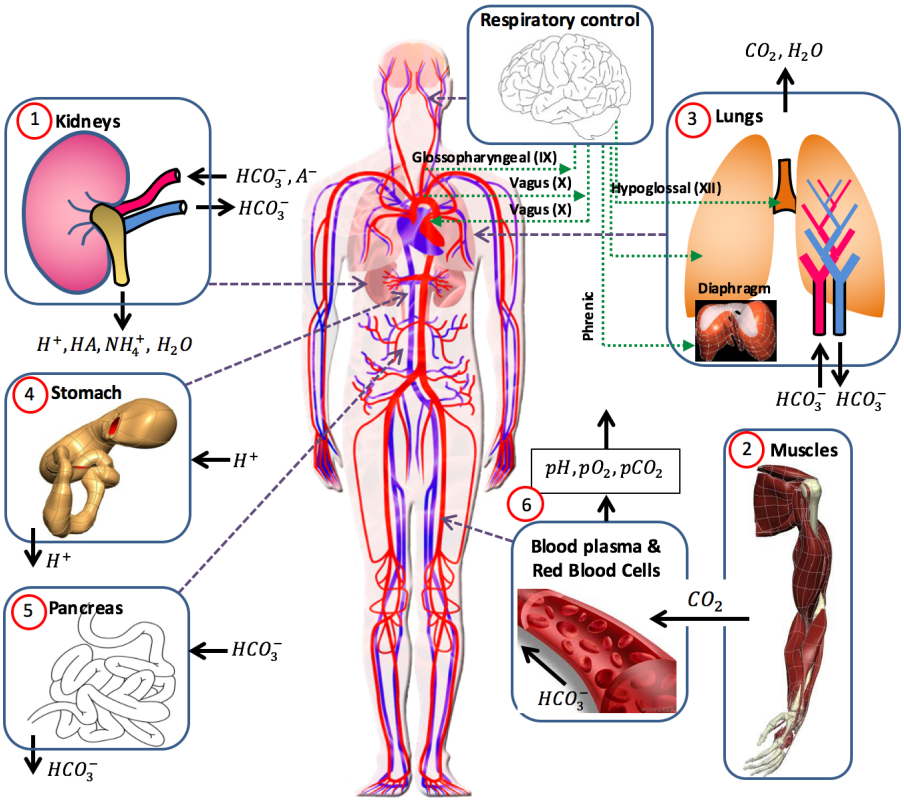

Figure 1: A whole body model containing organ level models for ion or gas exchange in the kidneys, muscles, lungs (with respiratory control), stomach, pancreas and systemic circulation.

that assumption later. Taking logs and using Henry's law, $[CO_2] = s.p_{CO_2}$, where s is the solubility coefficient for CO_2 in the relevant fluid, yields the Henderson-Hasselbalch equation for the CO_2/HCO_3^- buffer system:

$$pH = pK + \log \frac{[HCO_3^-]}{s.p_{CO_2}} \tag{1}$$

where $pH = -\log_{10}[H^+]$, $pK = -\log_{10} K$.[2]

Next, the buffering of H^+ by weak acids and weak bases occurs via two types of reaction[3]. The first is the dissociation of cationic weak acid (BH^+) to weak base (B), governed by the reaction

$$BH^+ \leftrightarrow B + H^+, \qquad e.g. \quad NH_4^+ \leftrightarrow NH_3 + H^+$$

Assuming a rapid equilibration, the governing equation for the model is

$$K_B = \frac{[B][H^+]}{[BH^+]} \tag{2}$$

Whether these buffers are sufficiently close to equilibrium to make this assumption is debatable [ref].

Similarly, dissociation of uncharged weak acid (HA) to anionic weak base (A^-) is governed by the reaction

[2] For arterial blood $pK \approx 6.1$, $HCO_3^- \approx 24$mM, $s = 0.03$mM/mmHg and $p_{CO_2} = 40$mmHg, giving $pH \approx 7.4$.

[3] Note that an acid or base (alkali) is any chemical substance that can donate or accept an H^+, respectively [1].

$$\mathrm{HA} \leftrightarrow \mathrm{A^-} + \mathrm{H^+}, \qquad e.g. \quad \mathrm{HCO_3^-} \leftrightarrow \mathrm{OH^-} + \mathrm{CO_2}$$

and at equilibrium

$$K_\mathrm{A} = \frac{[\mathrm{A^-}][\mathrm{H^+}]}{[\mathrm{HA}]} \tag{3}$$

These reactions hold on both sides of a cell membrane, with the same equilibrium constants on both sides. The neutral species (B and HA) move freely down their concentration gradients to equilibrate at equal concentration on either side of the membrane, as indicated in Figure 2. The charged species ($\mathrm{BH^+}$, $\mathrm{A^-}$ and $\mathrm{H^+}$), on the other hand, move down their concentration gradients (within a membrane protein channel) until equilibrating with their Nernst potentials,

$$E_\mathrm{BH} = \frac{RT}{F}\ln\frac{[\mathrm{BH^+}]_o}{[\mathrm{BH^+}]_i}, \qquad E_\mathrm{A} = \frac{RT}{F}\ln\frac{[\mathrm{A^-}]_o}{[\mathrm{A^-}]_i}, \qquad E_\mathrm{H} = \frac{RT}{F}\ln\frac{[\mathrm{H^+}]_o}{[\mathrm{H^+}]_i}.^4 \tag{4}$$

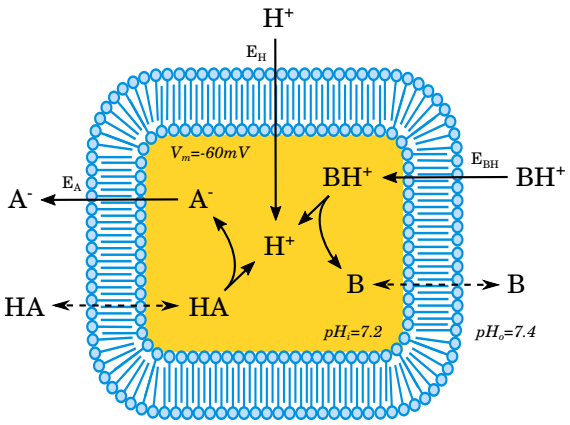

Figure 2: Movement of weak acids and weak bases across the cell membrane. The dotted lines indicate free movement of the uncharged species across the cell membrane. The solid lines indicate the flux of a charged species for which thermally driven diffusion equilibrates the concentration difference with the electrostatic charge difference (the Nernst equation).

Since the reaction $\mathrm{BH^+} \leftrightarrow \mathrm{B} + \mathrm{H^+}$ is in equilibrium on both sides of the membrane and both K_B and [B] are the same on both sides (free permeation of the uncharged molecule), from Equation (2)

$$K_B = \frac{[\mathrm{B}][\mathrm{H^+}]_o}{[\mathrm{BH^+}]_o} = \frac{[\mathrm{B}][\mathrm{H^+}]_i}{[\mathrm{BH^+}]_i}, \qquad or \qquad \frac{[\mathrm{H^+}]_o}{[\mathrm{H^+}]_i} = \frac{[\mathrm{BH^+}]_o}{[\mathrm{BH^+}]_i} \tag{5}$$

and therefore

$$E_{BH} = E_H. \tag{6}$$

On the other hand, since the reaction $\mathrm{HA} \leftrightarrow \mathrm{A^-} + \mathrm{H^+}$ is in equilibrium, and $[\mathrm{HA}]_o = [\mathrm{HA}]_i = [\mathrm{HA}]$, now we have

$$K_A = \frac{[\mathrm{A^-}]_o[\mathrm{H^+}]_o}{[\mathrm{HA}]} = \frac{[\mathrm{A^-}]_i[\mathrm{H^+}]_i}{[\mathrm{HA}]}, \qquad or \qquad \frac{[\mathrm{A^-}]_o}{[\mathrm{A^-}]_i} = \frac{[\mathrm{H^+}]_i}{[\mathrm{H^+}]_o} \tag{7}$$

and therefore

$$E_A = -E_H. \tag{8}$$

[4] $R \approx 8.4\mathrm{J.mol^{-1}.K^{-1}}$ and $F \approx 0.96e5\mathrm{C.mol^{-1}}$, therefore at $T = 298\mathrm{K}(25\mathrm{C})$, $RT \approx 2.5\mathrm{kJ.mol^{-1}}$ and $RT/F \approx 25\mathrm{mV}$.

There are many sources of H^+ flux across a cell membrane and we list the important ones for the current analysis below. If J_E is the rate of acid extrusion (generally at a metabolic cost) and J_L is the rate of acid loading, the difference between them drives the time rate of change of pH in the cell:

$$\frac{dpH_i}{dt} = \frac{\rho}{\beta}(J_E - J_L) \tag{9}$$

(called the fundamental law of pH_i regulation) where $\rho(m^{-1})$ is the surface to volume ratio of the cell, and β(mM/pH_unit) is the buffering power[5]. We consider an open system (the free exchange of energy and mass - in this case CO_2 - with the atmosphere) only, in which case β is $\beta_{open} = 2.3[HCO_3^-]$. Note that ρ/β has units of pH_unit.m^{-1}.mM^{-1}, J_E and J_L have units of mol.s^{-1}.m^{-2} (or mM.s^{-1}.m) and dpH_i/dt has units of pH_unit.s^{-1}.

For a particular cell the acid fluxes J_E and J_L are dependent on a range of protein exchangers, channels and pumps that reside in the cell membrane and are modelled individually. For the cells of interest here these are the acid extruding membrane transporters (NHE, NBC and NDCBE, all driven by the sodium gradient), the acid loading membrane transporters (NBCe1,2 and AE), and various leak channels and ATP-dependent pumps (such as HKA and V-type) shown individually in Figure 3. Note that NHE, NBC and NDCBE depend on the sodium gradient which must be maintained by the ATP-dependent sodium-potassium exchange pump NCX, but since we are not tracking sodium or metabolism, that pump is not included.

The equations governing these exchangers and pumps are provided on the CellML model repository. Most depend on carrier-mediated mechanisms, rather than simple diffusion gradients and therefore obey Michaelis-Menten kinetics where the steady state flux is given by

$$J_E = J_{max}\frac{[H^+]}{K_m + [H^+]}, \tag{10}$$

where J_{max} and K_m are constants. Here we assume that these models have already been established as CellML models in PMR - see, for example, https://models.physiomeproject.org/e/236/.

The cells of interest for the tissue level models below are a muscle cell, a renal epithelial cell, a gastric epithelial cell, a pancreatic epithelial cell, the red blood cell or RBC (treated as 3 cases: within the arterial system, within the capillary bed and within the venous system). For the tissue level models we define seven tissue compartments (see Figure 4): alveoli space; renal tubule; gastric interior; pancreas interior; and arterial, capillary and venous blood plasma.

Using these cell and tissue compartments, we now define ***composite multicellular tissue models*** for each of the six organ-level models (kidney, muscle, lung, stomach, pancreas and vascular system). Equation (9) is used with appropriate transporters for each parenchymal cell in the organ or organ system tissue model. In each case the parenchymal cells for each organ connect with blood plasma (arterial, capillary or venous). We later accumulate all exchange with blood plasma into one model for the arterial blood plasma, one for capillary blood plasma and one for venous blood plasma. Each model includes the variables shown to the right associated with each compartment. The inputs and outputs for each model are shown above and below the box with an inward or outward arrow, respectively.

Model 1: Kidney

There are several mechanisms to be considered in this model, as shown in Figure 5

[5] A buffer is any substance that tends to minimize changes in pH by reversely producing or consuming H^+. The buffering power of a solution is measured by the amount of added acid or base (per unit volume of solution) needed to decrease or increase the solution pH by one pH unit. *i.e.* a buffer with a high value of β requires a lot of additional acid or base to produce a unit change in pH. Without CO_2/HCO_3^-, the buffering power of whole blood is about 25mM/pH_unit (called the non-HCO_3^- buffering power). 80% of this non-HCO_3^- buffering power is associated with the cellular components of blood [1].

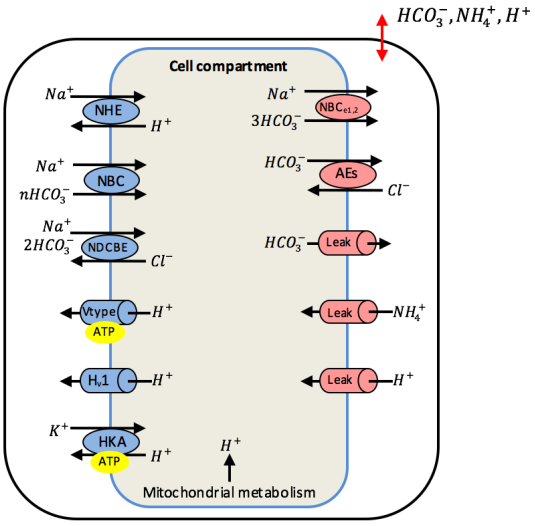

Figure 3: Membrane proteins (channels and transporters) divided into acid extruders (on the left) and acid loaders (on the right), shown here within a composite cell model. Note that the movement of ions across the cell membrane is driven by a sodium gradient (NHE, NBC, NDCBE), a chloride gradient (AE) or a metabolically dependent process (ATP label). Each channel and transporter is modelled with a separate CellML model on the PMR website.

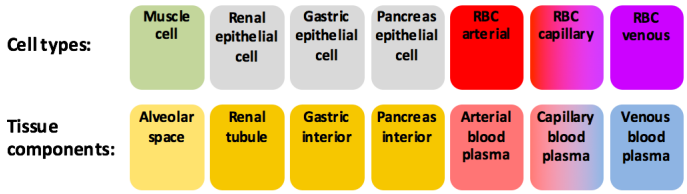

Figure 4: Cell and tissue compartments, to which variables and equations are assigned.

(a) One is the cellular mechanism of *HCO_3^- reabsorption* in the kidney. The HCO_3^- filtered by the glomerulus is combined with H^+ excreted from the epithelial cell (via the ATP-dependent H-pump and HKA pump, and the Na-dependent exchanger NHE) to form CO_2 and water (via the carbonic anhydrase reaction in the tubule) that diffuses back into the epithelial cell to then regenerate HCO_3^- in the blood (via the carbonic anhydrase reaction in the epithelial cell). The kidney reclaims virtually all filtered HCO_3^-.[6]

(b) The second is *ammonium excretion.* The kidney synthesizes NH_3/NH_4^+ as a urinary buffer to assist with the excretion of H^+. Filtered H^+ in the tubule titrates NH_3 excreted from the epithelial cell following glutamine metabolism (which produces both NH_4^+ and OH^-, thereby also generating new HCO_3^- into the blood). Conversion of the amino acid glutamine to urea and ammonia, is catalysed by glutaminase in both the liver and the kidney. Under conditions of blood acidosis, NH_4^+ excretion in the kidney is enhanced by up-regulating glutaminase production to increase NH_3 production, and glutaminase production is correspondingly down-regulated in the liver[7] .

(c) The third is *titratable acid formation.* When the excreted H^+ combines with filtered buffers other than HCO_3^- or ammonia, the outcome is the urinary loss of uncharged weak acid HA and the generation of new

[6] At 180L of filtered blood per day with $[HCO_3^-]$= 24mM, this is 4.32 moles of HCO_3^- per day [1].

[7] The liver also consumes glutamine for urea synthesis, and this is enhanced by an alkalosis-induced increase in glutaminase production in the liver.

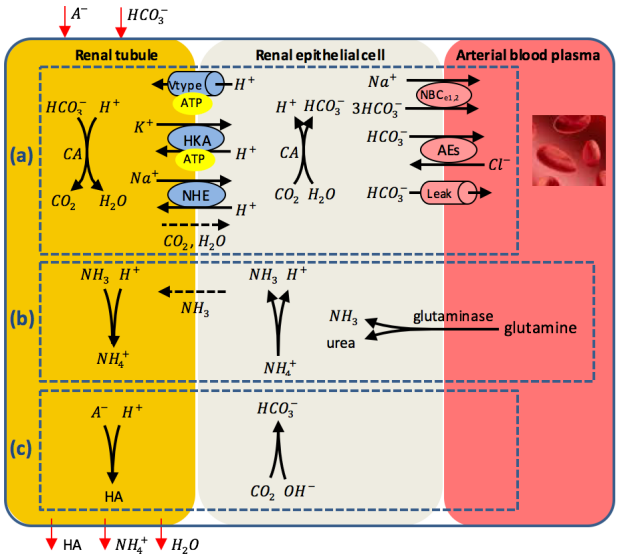

Figure 5: Cellular mechanisms in the kidney: (a) HCO_3^- reabsorption, (b) ammonium excretion, and (c) titratable acid formation.

HCO_3^- into the blood[8].

In formulating the equations for the kidney model, we assume that every HCO_3^- that is transported out of the epithelial cell to the blood plasma is immediately replaced with a H^+ from the CO_2 hydration reaction - *i.e.* there is no shortage of carbonic anhydrase and there is no shortage of CO_2 available to feed the reaction. This CO_2 is also assumed to diffuse with no delay from the renal tubule. Note that we are assuming the cell to be a well-stirred system. In reality there may be significant gradients of $[H^+]$ and $[HCO_3^-]$ particularly adjacent to transport proteins that influence the trans-membrane fluxes, but here we neglect the possible influence of unstirred layers.

Using sub- or superscripts *pt* for renal proximal tubule, *ec* for renal epithelial cell and *cb* for peritubular capillary blood to indicate which compartment a variable belongs to, the equations for this model are:

Renal proximal tubule

$$\frac{dpH_{pt}}{dt} = \frac{-\rho}{\beta_{CO_2}}(-J^{pt}_{HCO_3^-} + J^{NHE}_{H^+} + J^{Vtype}_{H^+} + J^{hyd}_{H^+}) \tag{11}$$

$$[H^+]_{pt} = 10^{-pH_{pt}} \tag{12}$$

Note that we are assuming that every H^+ transported to the renal tubule from the epithelial cell immediately combines with a filtered HCO_3^- to produce water and CO_2, which diffuses back to the epithelial cell to continue the cycle. In reality there may be pH gradients along the tubule created by diffusion or advection by urinary flow.

With $[H^+]$ now calculated on both sides of the apical (tubule-epithelial) membrane, the Nernst potential E_H can be calculated and therefore the ratio of NH_4^+ and OH^- concentrations on either side of the membrane:

[8] Note that about 70 mmole/day of new HCO_3^- is needed to neutralise the ~ 70 mmole/day of non-volatile acid - comprised of ~ 40 mmol/day of non-volatile acid produced (in addition to CO_2) by metabolism, ~ 20 mmol/day of dietary strong acid, and the intestinal loss of ~ 10 mmol/day of HCO_3^-. There must also be a corresponding excretion of ~ 70 mmol/day of H^+ into the urine [2].

$$E_{\mathrm{H}} = \frac{RT}{F} \ln \frac{[\mathrm{H}^+]_{pt}}{[\mathrm{H}^+]_{ec}} \tag{13}$$

$$\frac{RT}{F} \ln \frac{[\mathrm{NH}_4^+]_{pt}}{[\mathrm{NH}_4^+]_{ec}} = E_{\mathrm{H}} \tag{14}$$

$$\frac{RT}{F} \ln \frac{[\mathrm{OH}^-]_{pt}}{[\mathrm{OH}^-]_{ec}} = -E_{\mathrm{H}} \tag{15}$$

Renal epithelial cell

$$\frac{dpH_{ec}}{dt} = \frac{-\rho}{\beta}(-J_{\mathrm{H}^+}^{NHE} - J_{\mathrm{H}^+}^{Vtype} + 3.J_{\mathrm{HCO}_3^-}^{NBC} + J_{\mathrm{H}^+}^{hyd} + J_{\mathrm{HCO}_3^-}^{leak} + J_{\mathrm{H}^+}^{source}) \tag{16}$$

$$[\mathrm{H}^+]_{ec} = 10^{-pH_{ec}} \tag{17}$$

Note that the flux terms J in Equation 16 are positive in the direction of the arrows in Figure 5 - *i.e.* a positive flux of H^+ from the epithelial cell to the renal tubule and a positive flux of HCO_3^- from the epithelial cell to the capillary. The factor of 3 for the NBC transporter reflects the transfer of $3HCO_3^-$ ions for every one Na^+. The term $J_{\mathrm{H}^+}^{source}$ includes all sources of H^+ production within the cell. Note that p_{CO_2} is constant across all three renal compartments.

Arterial blood plasma

$$\frac{dpH_{cb}}{dt} = \frac{-\rho}{\beta}(-3.J_{\mathrm{HCO}_3^-}^{NBC} + J_{\mathrm{H}^+}^{hyd} - J_{\mathrm{HCO}_3^-}^{leak} + J_{\mathrm{HCO}_3^-}^{sink}) \tag{18}$$

The bicarbonate sink term in this equation is considered later when we model CO_2 and HCO_3^- exchange with the RBCs.

Model 2: Muscle

Myocyte

$$\frac{dpH_{myo}}{dt} = \frac{\rho}{\beta}(3.J_{\mathrm{HCO}_3^-}^{NBC} + J_{\mathrm{HCO}_3^-}^{AE} + J_{\mathrm{HCO}_3^-}^{leak}) \tag{19}$$

Capillary blood plasma

$$\frac{dpH_{cb}}{dt} = \frac{\rho}{\beta}(3.J_{\mathrm{HCO}_3^-}^{NBC} + J_{\mathrm{HCO}_3^-}^{AE} + J_{\mathrm{HCO}_3^-}^{leak} - J_{\mathrm{HCO}_3^-}^{cb-sink}) \tag{20}$$

Metabolic activity in muscle produces CO_2 which diffuses across the cell membranes to the capillary blood, or the CO_2 is converted to bicarbonate and actively transported, as illustrated in Figure 6.

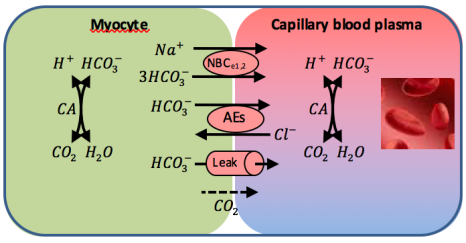

Figure 6: The release of CO_2 from metabolic activity in muscle into the blood stream.

The bicarbonate sink term in this equation is considered later when we model CO_2 and HCO_3^- exchange with the RBCs.

Model 3: Lungs & Respiratory Control

There are several ways to develop a model for gas exchange between the pulmonary capillaries and alveolar air. One approach is to develop a detailed biophysical model that takes into account the anatomy and material properties of all the cells and tissues that influence the diffusion of O_2 and CO_2 (see [1] for a detailed discussion of this). Another, more empirical, approach is to represent the volume rate of transport of CO_2 across the lung endothelium from capillary to alveolar space[9] with Fick's law using a proportionality constant that takes into account the cross-sectional area and length of the diffusion path and the molecular weight of the gas:

$$\dot{V}_{CO_2} = k\frac{A.s}{h\sqrt{MW}}(p^a_{CO_2} - p^c_{CO_2}) \tag{21}$$

where A (m^2) is the surface area for gas exchange, h (m) is the distance between the alveolar space and the blood plasma, s (0.03 mM/mmHg or 0.03 $mol.m^{-3}.mmHg^{-1}$) is the solubility of CO_2 in the tissue, MW is molecular weight (44 for CO_2) and k is a proportionality constant [1]. $p^a_{CO_2}$ and $p^c_{CO_2}$ are the alveolar and capillary partial pressures of CO_2 (mmHg).

The nerves involved in respiratory control are shown in Figure 1 by green dashed lines. Blood gases (CO_2, O_2 and pH) are sensed peripherally by glomus cells in the carotid and aortic bodies at the bifurcation of each of the common carotid arteries and in the aortic arch, respectively, and send feedback signals to the medulla via afferents of the glossopharyngeal nerve (CN IX) and the vagus nerve (CN X), respectively. They respond to hypoxia, hypercapnia and acidosis. Other so-called central chemoreceptors are located within the brain parenchyma in brain extracellular fluid behind the blood-brain barrier. These appear to be responsible for 65-80% of the integrated response but with a slower time constant than the faster acting peripheral receptors. The end result of this feedback is modulation of a respiratory rhythm generator in the medulla that controls the inspiratory phase of breathing via the phrenic nerve output to the respiratory muscles. Lung movement is mainly controlled by the diaphragm, which is excited during inspiration by a signal from the phrenic nerve. It recoils during expiration which is usually passive in mammals, although forced expiration can be induced by the abdominal muscles. The resistance to flow in the upper airway and movements of the tongue are affected by signals from the hypoglossal nerve. The vagus nerve is an important bundle of nerves that carries signals to and from the brainstem. Signals from chemoreceptors and baroreceptors in the aorta as well as signals from stretch receptors in the lungs are transferred via the vagus nerve to the brainstem, and signals that act to slow the heart rate are transferred by the vagus nerve to the heart. Chemoreceptors and baroreceptors are also located in the carotid sinus and their signals are transferred to the brainstem via the glossopharyngeal nerve. The lung itself is a complex organ that comprises of airways and blood vessels that are âĂŸsuspendedâĂŹ within a delicate network of gas exchange tissue4. The airways, pulmonary arteries, and pulmonary veins converge at the alveoli (microscopic airfilled sacs, with walls comprised of capillaries) where respiratory gas exchange occurs.
For the purposes of the present whole body acid-base model we will ignore the details of both gas exchange on the lungs and the feedback control of respiration and just define an empirical relationship between ventilation and blood gas concentrations. This is discussed in [1] and shown in Figure 7 as plots of total ventilation (in $L.min^{-1}$) as a function of (a) $p^a_{CO_2}$ and (b) $p^a_{O_2}$.

Model 4: Stomach

The acidic environment in the stomach ($pH \approx 2$), required to kill bacteria and to aid food breakdown, is maintained by the H^+/K^+-ATPase pump in parietal cells lining the stomach, as shown in Figure 8.

[9] A 70 Kg person on a typical western diet produces ~ 15 mol/day or 0.66 Kg/day of CO_2 from metabolism.

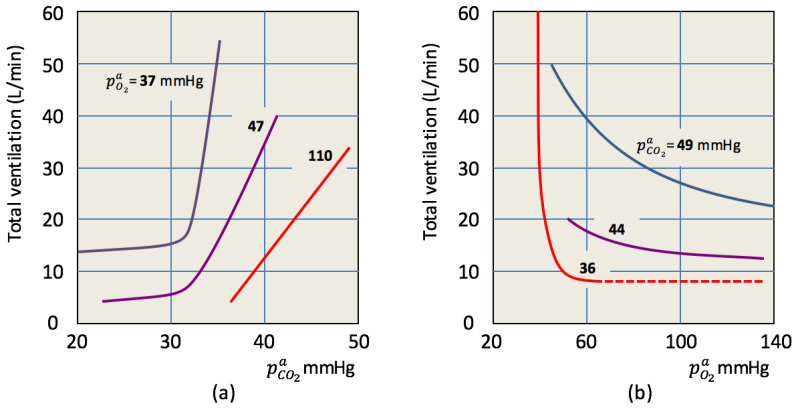

Figure 7: Integrated ventilatory responses to changes in (a) $p^a_{CO_2}$ and (b) $p^a_{O_2}$ (adapted from [1]).

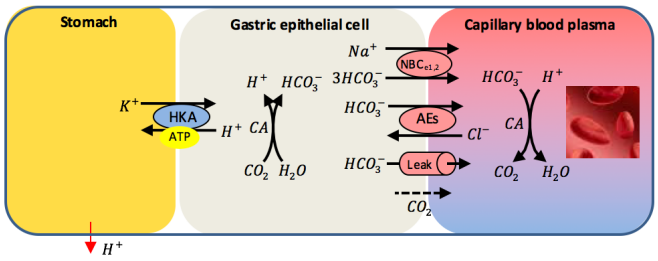

Figure 8: Release of H^+ via the H^+/K^+-ATPase in parietal cells of the stomach.

The acid produced by parietal cells in the stomach has to be neutralised for chyme arriving in the duodenum. This is achieved via the release of cholecysto-kinase (CCK) from ... which stimulates the release of HCO_3^- from S-cells in the pancreas.

Model 5: Pancreas

Pancreas

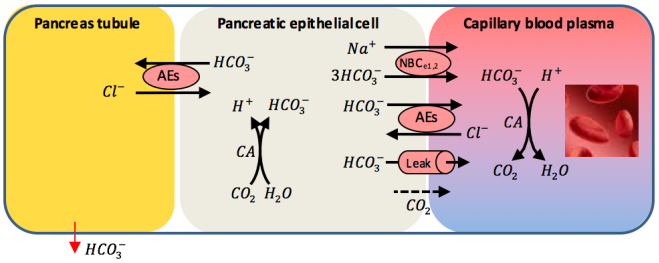

Figure 9: Release of HCO_3^- via the HCO_3^-/Cl^- exchanger in S-cells of the pancreas.

Model 6: Blood Circulation

We treat the arterial circulation as one homogenous compartment and the venous circulation as another separate homogenous compartment, in order to allow for the differences in arterial and venous concentrations of CO_2, HCO_3^- and H^+.

Exchange of CO_2 and HCO_3^- between plasma and red blood cells

The vascular transport of muscle-generated CO_2 or recycled HCO_3^- from the kidney depends heavily on the gas-channel mediated transport of CO_2 from plasma to red blood cells where it is hydrolysed to HCO_3^-, dissolved or stored as carbamino hemoglobin (Hb_NH_COO$^-$) via the reaction

$$\text{Hb\_NH}_2 + \text{CO}_2 \leftrightarrow \text{Hb\_NH\_COO}^- + \text{H}^+$$

within the RBC. Assuming equilibrium,

$$K_H = \frac{[\text{Hb\_NH\_COO}^-]_{rbc}.10^{-pH_{rbc}}}{[\text{Hb\_NH}_2 + \text{CO}_2]_{rbc}} \tag{22}$$

Similarly in the RBC, $HCO_3^- \leftrightarrow OH^- + CO_2$ at equilibrium gives

$$K_A = \frac{s.p_{CO2}.[\text{OH}^-]_{rbc}}{[\text{HCO}_3^-]_{rbc}} \tag{23}$$

And in the plasma

$$pH_{plasma} = pK + \log \frac{[\text{HCO}_3^-]_{plasma}}{s.p_{\text{CO}_2}} \tag{24}$$

As indicated in Figure 9, nearly 70% of the newly generated is carried away in the blood stream as bicarbonate (mostly in the RBC) about 20% as carbamino haemoglobin and only 10% in solution.

Note that the significance of membrane transporters such as the Rh complex and AQP1 for CO_2 is controversial (RVJ ref) since diffusion delays in the unstirred layers adjacent to the membrane may be as important as the kinetics of the membrane transporters. The RBC membrane is unusual in being crammed with proteins that limit the area of bilipid membrane available for CO_2 diffusion, so it is possible that membrane protein-facilitated transport may be more significant here than in other cell types (ref). We ignore these subtleties here and just assume an unimpeded rapid transfer of CO_2 across the RBC membrane.

Note also that here we are not dealing with the Bohr effect (the enhanced release of O_2 from haemoglobin through CO_2 binding) or the movement of water to supply OH^- for bicarbonate production in the RBCs (and their consequent swelling) in the systemic capillaries, but both effects may be readily added to the model.

Composite Model

References

[1] Walter F Boron and Emile L Boulpaep. *Medical physiology*. Elsevier Health Sciences, 2016.

[2] Rossana Occhipinti and Walter F Boron. Mathematical modeling of acid-base physiology. *Progress in biophysics and molecular biology*, 117(1):43–58, 2015.

[3] Walter F Boron. Regulation of intracellular pH. *Advances in physiology education*, 28(4):160–179, 2004.

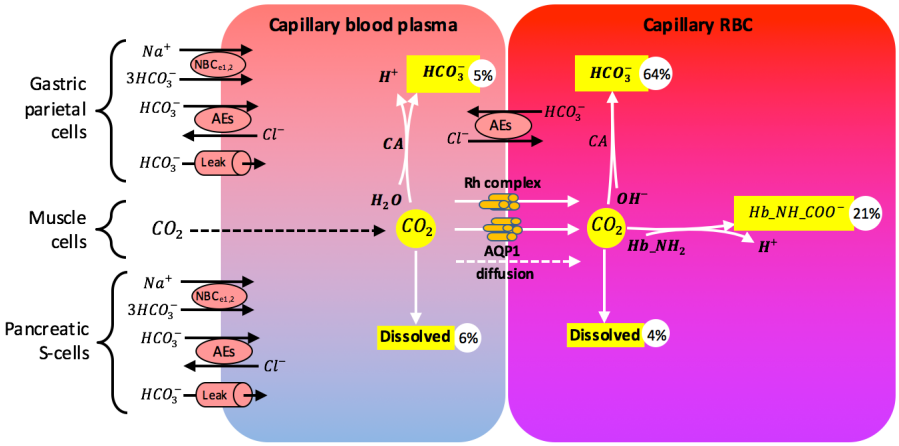

Figure 10: Exchange of CO_2, HCO_3^- and H^+ between parenchymal cells and plasma and between plasma and red blood cells. CO_2 is transported to the RBC by diffusion (dotted line) and via membrane protein channels (Rh complex and AQP1). CO_2 is stored as HCO_3^-, $Hb\_NH\_COO^-$ or in solution.

[4] Walter F Boron. Sharpey-schafer lecture: Gas channels. *Experimental physiology*, 95(12):1107–1130, 2010.

[5] Walter F Boron and Paul De Weer. Active proton transport stimulated by CO_2/HCO_3^-, blocked by cyanide. 1976.

[6] Walter F Boron and Paul De Weer. Intracellular pH transients in squid giant axons caused by CO_2, NH_3, and metabolic inhibitors. *The Journal of General Physiology*, 67(1):91–112, 1976.

[7] Erkki Somersalo, Rossana Occhipinti, Walter F Boron, and Daniela Calvetti. A reaction-diffusion model of CO_2 influx into an oocyte. *Journal of theoretical biology*, 309:185–203, 2012.

[8] Rossana Occhipinti, Raif Musa-Aziz, and Walter F Boron. Evidence from mathematical modeling that carbonic anhydrase II and IV enhance CO_2 fluxes across Xenopus oocyte plasma membranes. *American Journal of Physiology-Cell Physiology*, 307(9):C841–C858, 2014.

[9] Francisco C Villafuerte, Pawel Swietach, Jae-Boum Youm, Kerrie Ford, Rosa Cardenas, Claudiu T Supuran, Philip M Cobden, Mala Rohling, and Richard D Vaughan-Jones. Facilitation by intracellular carbonic anhydrase of Na^+-HCO_3^- co-transport but not Na^+/H^+ exchange activity in the mammalian ventricular myocyte. *The Journal of physiology*, 592(5):991–1007, 2014.

[10] Alzbeta Hulikova and Pawel Swietach. Rapid CO_2 permeation across biological membranes: implications for CO_2 venting from tissue. *The FASEB Journal*, 28(7):2762–2774, 2014.

[11] Pawel Swietach, Chae-Hun Leem, Kenneth W Spitzer, and Richard D Vaughan-Jones. Pumping Ca^{2+} up H^+ gradients: A Ca^{2+}-H^+ exchanger without a membrane. *The Journal of physiology*, 592(15):3179–3188, 2014.

[12] Pawel Swietach, Massimiliano Zaniboni, Andrew K Stewart, Alessandra Rossini, Kenneth W Spitzer, and Richard D Vaughan-Jones. Modelling intracellular H^+ ion diffusion. *Progress in biophysics and molecular biology*, 83(2):69–100, 2003.

[13] Leila V Virkki, Darren A Wilson, Richard D Vaughan-Jones, and Walter F Boron. Functional characterization of human NBC4 as an electrogenic Na^+-HCO_3^- cotransporter (NBCe2). *American Journal of Physiology-Cell Physiology*, 282(6):C1278–C1289, 2002.

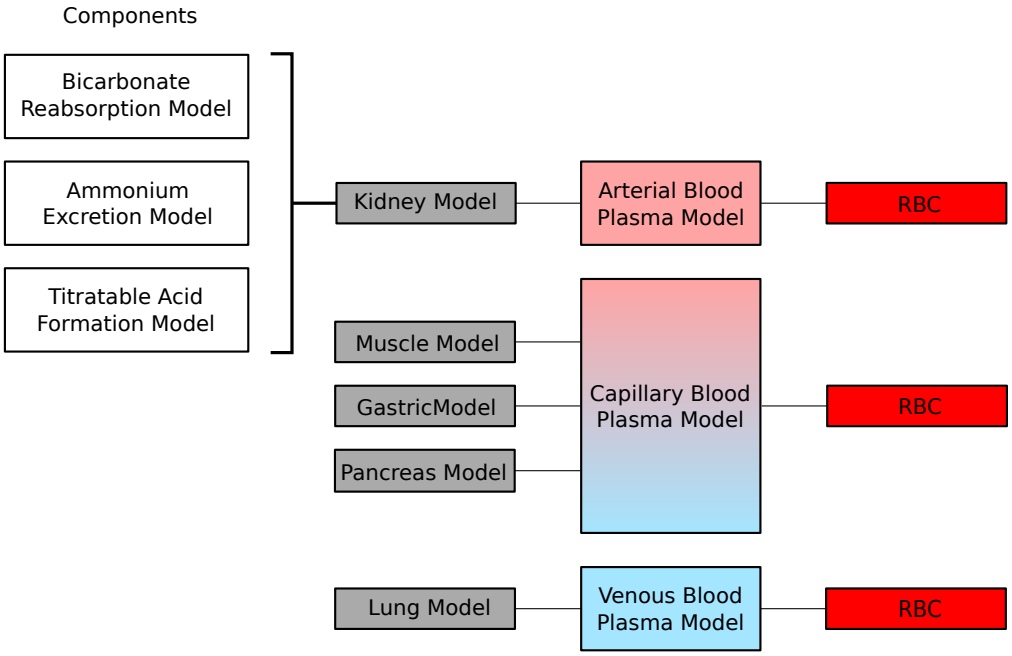

Figure 11: Block diagram showing how models relate to each other.